Biomaterials Science

ROYAL SOCIETY OF CHEMISTRY

PAPER

View Article Online
View Journal | View Issue

Open Access Article. Published on 15 September 2025. Downloaded on 3/12/2026 6:43:35 PM.
This article is licensed under a Creative Commons Attribution 3.0 Unported Licence.

Check for updates

Cite this: *Biomater. Sci.*, 2025, **13**, 5741

Double-network polysaccharide hydrogel for guided tissue repair†

Mathilde Maillard, Chloé Dujardin, Paola Aprile, Rachida Aid, Didier Letourneur and Teresa Simon-Yarza *

Received 22nd January 2025,
Accepted 29th March 2025

DOI: 10.1039/d5bm00117j

rsc.li/biomaterials-science

The increasing need for biocompatible and sustainable materials has highlighted the potential of natural-based polymers in tissue engineering, particularly due to their bioactivity, degradability, and ability to mimic the extracellular matrix. Polysaccharide-based membranes are especially promising for guided tissue regeneration (GTR) applications, thanks to their biocompatibility, resorbability, and capacity to recreate biological environments. However, their limited mechanical properties present challenges for practical handling during implantation. In this study, double-network polysaccharide hydrogels were developed to enhance the mechanical robustness of polysaccharide membranes for tissue engineering purposes. By optimizing synthesis parameters, a biphasic membrane was achieved, comprising a non-porous side to serve as a physical barrier and a porous side to facilitate cellular infiltration during GTR. Sterilization *via* gamma irradiation did not compromise the structural integrity or implantability of the membranes. Furthermore, *in vivo* studies using a mouse subcutaneous model demonstrated a barrier effect, confirming the suitability of these membranes for guided tissue repair. These findings demonstrate the potential of engineered polysaccharide membranes as versatile and effective materials in regenerative medicine.

Introduction

The development of new materials for tissue engineering applications remains a challenge, driven by the need to balance specific biological and mechanical properties. Natural-based polymers have demonstrated numerous advantages compared to synthetic polymers. The principal limitations of synthetic polymers used in guided tissue regeneration (GTR) involve poor mechanical properties, inadequate degradation *in vivo*, pernicious foreign body response, lack of bioactivity, excessive cost and regulatory issues.[1–3] Collagen, the main component of the extracellular matrix (ECM), is currently used clinically. To improve its mechanical properties, collagen is frequently cross-linked using physical, chemical and enzymatic methods, resulting also in longer resorption times. A major drawback of collagen is its animal origin, which is associated with undesired immune responses and complicated regulatory processes. Polysaccharide-based materials, major components of the ECM too, are already widely described in the literature. Based on their numerous advantages, such as their biocompatibility due to their natural non-animal origin, resorbability properties, availability and cost-effectiveness, several products have already been commercialized for tissue repair.[4–6]

Polysaccharides are versatile polymers that can be shaped using different strategies, such as molding or 3D printing, offering a broad range of designs that result in a variety of applications. Additionally, there is a plethora of polysaccharides available, allowing for the targeting of specific biological, physical, and chemical characteristics at a relatively low cost.[5,7–13] In this context, polysaccharide membranes have demonstrated significant potential for GTR, due to their barrier function that prevents cell infiltration into bone defects while preserving the remodelling of bone tissue.[14–16]

Despite their proven benefits, polysaccharide-based membranes face challenges due to their poor mechanical properties and their fast degradation rate.[17,18] In a recent work, we demonstrated the potential of novel porous biodegradable membranes composed of polysaccharides, specifically pullulan and dextran, for guided bone regeneration (GBR) membranes.[15] While these membranes have shown good biocompatibility and *in vivo* osteoinductive properties comparable to those of commercially available collagen membranes, they have suffered from insufficient mechanical strength and slow degradation rates, which pose challenges for clinical use. To address these issues, strategies such as the combination with a

Université Paris Cité, Université Sorbonne Paris Nord, Laboratory for Vascular Translational Science (LVTS), INSERM U1148, 75018 Paris, France.
E-mail: teresa.simon-yarza@inserm.fr

† Electronic supplementary information (ESI) available. See DOI: https://doi.org/10.1039/d5bm00117j

Open Access Article. Published on 15 September 2025. Downloaded on 3/12/2026 6:43:35 PM.
This article is licensed under a Creative Commons Attribution 3.0 Unported Licence.

second material to create composite hydrogels have been investigated.[19,20] A range of studies have explored the potential of interpenetrating polymer networks (IPNs) to reinforce polysaccharide networks. These studies demonstrated that IPNs can lead to increased storage modulus assuring structural maintenance.[21] IPNs have led to promising materials in terms of biocompatibility and the promotion of blood vessel formation.[22,23] The insightful design of hydrogels with tailored properties based on IPNs has been recently reviewed.[24]

Amongst IPNs, double-network (DN) hydrogels are composed of two contrasting networks, typically a rigid first network and a soft second network, which contribute to their high strength and toughness.[25,26] The first network mainly serves to increase elastic modulus with sacrificial bonds, while the second one sustains stress and can be extended so as to increase the strain.[27] The combination of high mechanical strength and cytocompatibility makes DN hydrogels particularly interesting candidates for load-bearing tissue engineering applications, such as in cartilage regeneration or bone repair.[28]

One of the well-known polymers used for DN hydrogels is alginate. Alginate is a natural polysaccharide that can form strong cross-linkages in the presence of divalent ions. Biocompatibility, biodegradability and viscoelastic properties (strain-stiffening behaviour) make this material an excellent option to improve the mechanical properties of polysaccharide hydrogels for tissue engineering. The physical cross-linking allows for obtaining reversible/dynamic bond formation and also confers the ability to dissipate energy when breakage and reformation occur.[29] Moreover, it is a material that can be tuned to control physical cross-linking and gelation. Since it is biologically inert, it appears as a good candidate to produce materials intended for barrier functions, such as guided tissue regeneration membranes.[30,31]

Based on this, we have developed in this study several types of pullulan/dextran membranes for GTR following the DN strategy. In particular, we have assessed the physical and mechanical properties of pullulan/dextran membranes, and of membranes composed of a network of chemically cross-linked pullulan/dextran and a second network obtained by the addition of a third polysaccharide, namely alginate (Fig. 1). Moreover, we explored the effects of key manufacturing processes, including freeze-drying and sterilization, on these properties in view of their clinical implantation.

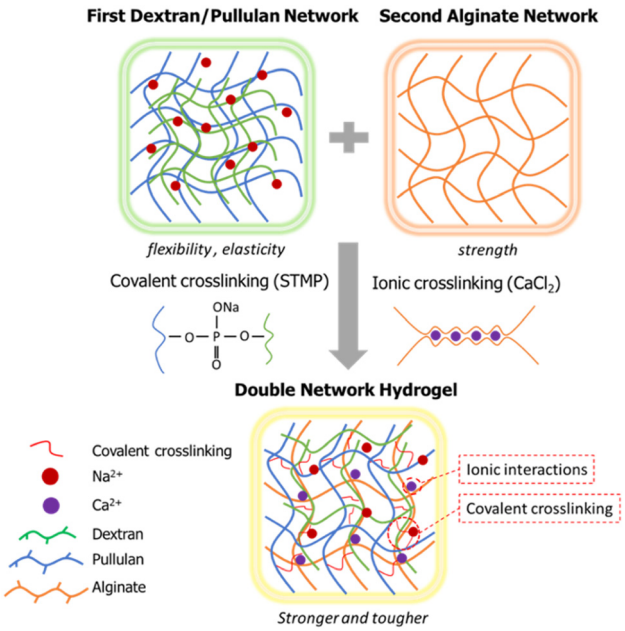

Fig. 1 Components of the polysaccharide-based membrane and contribution to the double network.

Experimental

Formulation of polysaccharide solutions

PuD, PuD-NaCl and PuDAlg-NaCl stand for pullulan-dextran, pullulan-dextran-NaCl and pullulan-dextran-alginate-NaCl, respectively.

Membranes were made up of pullulan (M_w = 200 kDa, Hayashibara, Japan) and dextran (M_w = 500 kDa, Pharmacosmos, Denmark). The molecular weights of pullulan and dextran used in this study result from previous works by the team.[32] NaCl (Fischer Chemical, USA) was used to decrease the hydrogel swelling.[33] For PuD-NaCl and PuDAlg-NaCl membranes with 75%–25% pullulan/dextran, 11.75 g of pullulan, 3.25 g of dextran, and 6 g of NaCl, were placed in a 100 mL beaker and mixed manually with a spatula. For PuDAlg-NaCl, 4 g of low viscosity alginate (Sigma Aldrich) was added. Then, 40 mL of deionized water was added, and the solution was stirred using a magnetic stirrer for 2 h at 200 rpm at room temperature. The different compositions of the membranes are summarized in Table 1.

Cross-linking and molding

Chemical cross-linking of polysaccharides was carried out in accordance with a method previously described.[34] Briefly, a solution of 2.25% w/v of trisodium trimetaphosphate (STMP, $Na_3O_9P_3$, Sigma-Aldrich) was added to a pullulan/dextran solution (10 g) in an alkaline environment (1 mL of 10 M NaOH). Then, the solution was placed into a 15 mL syringe and injected through a custom mould as illustrated in Fig. 2. The mould consisted of two plastic plates (10 mm length, 8 mm width) separated by a 0.3 mm-thick spacer (samples for rheology were set at 1 mm thickness). Incubation for 30 min at 50 °C was performed to complete the cross-linking process. Concerning the membrane with alginate (PuDAlg-NaCl), a second cross-linking was done by immersing the membrane in a bath of $CaCl_2$ (Sigma Aldrich) at 3% (w/v) for 30 min at room temperature. To stop the reaction, the pH of the hydrogel was neutralized using a buffer prepared by adding 2.5 mL of 1 M H_3PO_4 to 0.6 L of 0.7% ammonium bicarbonate $(NH_4)HCO_3$ (%w/w) for 30 min. This step was repeated four times.

 This journal is © The Royal Society of Chemistry 2025

Open Access Article. Published on 15 September 2025. Downloaded on 3/12/2026 6:43:35 PM.
This article is licensed under a Creative Commons Attribution 3.0 Unported Licence.

Table 1 Raw materials used in the formulations of PuD, PuD-NaCl and PuDAlg-NaCl membranes with a 75 : 25 pullulan/dextran ratio

Components	Function	PuD – mass [g] for 20 mL of polymeric solution	PuD-NaCl – mass [g] for 20 mL of polymeric solution	PuDAlg-NaCl – mass [g] for 20 mL of polymeric solution
Pullulan	Elasticity	5.625	5.625	5.625
Dextran	Rigidity	1.875	1.875	1.875
Sodium trimetaphosphate (STMP) – 2.5% w/v	Crosslinker	2	2	2
Alginate low viscosity	Double network	—	—	4
Calcium chloride ($CaCl_2$) – 3% w/v	Crosslinker	—	—	1
Sodium chloride (NaCl)	Gel property modifier	—	6	6
Sodium hydroxide (NaOH)	pH controller	2	2	2

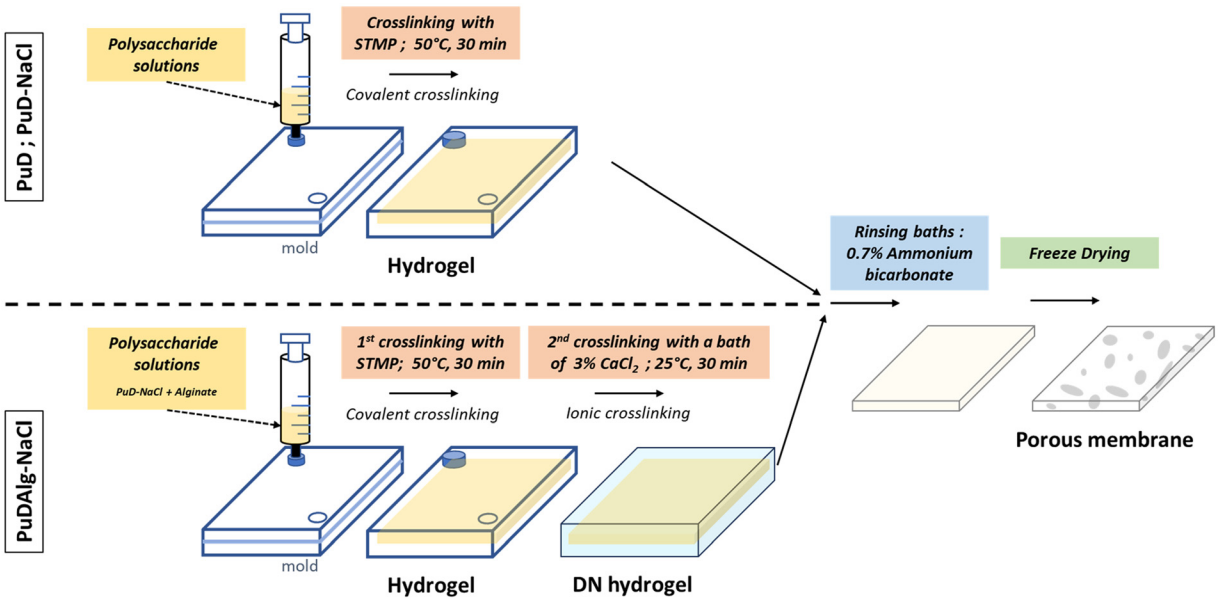

Fig. 2 Formulation and shaping of pullulan–dextran membranes. The DN hydrogel was obtained by a double network with alginate.

Freeze-drying

To obtain porous membranes, the cross-linked membranes were placed on a polystyrene Petri dish (Corning®) and loaded on freeze-dryer trays (S-FD, Pilot −80 freeze dryer, Cryotec®, France). The following protocol was applied: (1) freezing speed was fixed at −1 °C min^{-1} until reaching −35 °C and maintained for 1 h; (2) under a pressure of 0.05 mbar, primary drying (sublimation phase) was done by increasing the temperature from −35 °C to −5 °C at a speed rate of 0.1 °C min^{-1}; and (3) a second drying process was performed for 8 h at −5 °C and 0.05 mbar.

Macrostructural characterization

Macroporosity and topography of the membranes were assessed by scanning electron microscopy (SEM) using an FEI TeneoVS instrument (ImagoSeine facility, Jacques Monod Institute and LVTS, Paris). The membrane was cut in half using a razor blade, glued onto a carbon patch on each side or on the section to observe either the surface or the inner structure. The macrograph analysis was carried out under low vacuum mode (40 Pa) at a 5 kV acceleration voltage. The working distance was fixed at 10–12 mm and a low vacuum state was required to well observe the polysaccharide membrane. The porosity was then analysed using ImageJ software using thresholds and image analysis. All measurements were performed at room temperature, 24 h after the freeze-drying process.

Sterilization

The impact of sterilization based on γ-rays at 25 kGy on the physical and biological properties of the membranes was assessed and compared to that following irradiation using ultraviolet light at a wavelength of 254 nm for 1 h.

Swelling ratio

First, the dry weight of the membrane was measured. Membranes were hydrated in a 0.9% NaCl bath for 24 h. After immersion in 0.9% NaCl, the wet weight of the membrane was

Open Access Article. Published on 15 September 2025. Downloaded on 3/12/2026 6:43:35 PM.
This article is licensed under a Creative Commons Attribution 3.0 Unported Licence.

recorded every 5 min until reaching equilibrium. At each time point, the excess amount of liquid was carefully removed, and the membrane was weighed to determine its swelling ratio using the following equation:

$$S_w = \frac{(W_s - W_i)}{W_i} \quad (1)$$

where S_w is the swelling ratio, W_s is the mass of the swollen membrane and W_i is the mass of the dried membrane.

Enzymatic degradation

The *in vitro* degradation rate of the polysaccharide membrane was determined using a mixture of pullulanase and dextranase as previously reported.[35] These enzymes, produced by microorganisms, have been chosen to assure accelerated degradation of the materials for comparison between the formulations. A solution of 10% (v : v) of pullulanase and 5% (v : v) of dextranase was prepared in PBS. Culture Transwell® inserts (with pore sizes of 8 μm, PET track-etched membrane, 24-well plate format, Falcon) were first weighted. Freeze-dried membranes were then placed in the inserts and weighted with the Transwell. They were incubated at 37 °C in the enzymatic solution, and their weight was recorded every 5 min until the complete degradation of the sample (100% mass loss).

Phosphorus assessment

Phosphorus content was quantified according to a colorimetric method,[36] and we notably compared the impact of the STMP cross-linking temperature (25 °C or 50 °C). Three replicates of 20 mg of samples were immersed in 1 mL of 10% nitric acid at 105 °C for 3 h. Then, 0.4 mL of 14.7 M nitric acid, 2 mL of 10 mM ammonium metavanadate and 2 mL of 40 μM ammonium pentaphosphoric acid molybdate were added to the scaffold lysates. The phosphorus content was determined according to a calibration curve based on phosphoric acid and read using a microplate reader (Infinite® 200 PRO, Tecan) at 405 nm.

Rheology

The viscoelastic properties of the materials after cross-linking and after the freeze-drying process were investigated using a Discovery HR-2 rheometer (TA Instrument). Parallel-plate geometry was used (diameter = 4 cm, gap = 1 mm) at a frequency of 1 Hz and a shear strain of 0.1% (to reach the linear domain or the LVEC) with an axial force lower than 0.1 N. The gap of 1 mm was selected in order to create similar conditions to those during the moulding process (around 1 mm between plates). Both freeze-dried and non-freeze-dried samples were analysed and were incubated for 3 days in 0.9% NaCl prior to the analysis.

Viscoelastic properties, and particularly the complex modulus G^* [Pa], have been calculated by following the elasticity law described as follows:[37,38]

$$G^* = \frac{\tau_A}{\gamma_A} \quad (2)$$

with G^* denoting the complex shear modulus [Pa], τ_A denoting the shear stress amplitude [Pa] and γ_A denoting the strain amplitude [dimensionless]. This equation describes the viscoelastic behaviour of the material with storage modulus (G') also known as elastic modulus, and loss modulus (G'') often called viscous modulus:

$$(G*)^2 = G'^2 + G''^2 \quad (3)$$

Seeding of human gingival fibroblast cells and cytotoxicity assay

Cytocompatibility of the pullulan/dextran membrane was assessed with live and dead and indirect cytotoxicity assays following the ISO standard 10993-5:200931.[39] Human gingival primary cells (passage 6, P10866, Innoprot, Derio, Spain) were plated at 5×10^3 cells per cm^2, on T75 flasks with high glucose DMEM (Dulbecco's Modified Eagle's Medium; Thermo Fisher Scientific) supplemented with glutamax (2% FBS, 1% P/S and growth factor). Once 80% of confluence was reached, cells were used for live and dead and metabolic activity assays as follows: membrane disks of 8 mm treated by UV irradiation (254 nm) for 1 h. Membranes were then placed in 24-well sterile plates for the live and dead (non-cell culture-treated) assay, or into Transwell inserts for the cell viability assay.

For the cell viability indirect assay, materials were immersed in a cell culture medium for 24 h, and then the medium was collected to treat cells seeded on a 24-well cell culture plate at a density of 5×10^4 cells per well (Thermo Fisher Scientific). Samples were analysed at days 1, 3 and 7 with a CCK-8 viability assay following the manufacturer's protocol. Controls were prepared by treating cells with the cell culture medium under the same conditions but with no contact with the materials. Absorbance readings were taken at 490 nm and 690 nm using a microplate reader (Infinite® 200 PRO, Tecan) as per the manufacturer's instructions.

To investigate the barrier function of the membranes, cells were seeded on top of the membrane samples (smooth side or rough side) at a density of 25×10^4 cells per sample in 15 μL of the culture medium. The cells were allowed to be adsorbed for 30 min at 37 °C and under 5% CO_2, and then 200 μL of the medium was added every 15 min until a volume of 700 μL was reached. After 48 h of incubation at 37 °C and under 5% CO_2, the samples were washed with PBS and incubated for 30 min with a solution of the cell medium with the addition of ethidium-1 (4 μM final concentration, Sigma) and calcein (2 μM final concentration, EB-Biosciences). The staining solution was replaced by PBS for the following confocal microscopy analysis.

Confocal microscopy

To observe the porosity of the rehydrated membranes and the absence of cell migration due to the barrier function, fluorescent membranes were prepared with the addition of 5 mg of fluorescein isothiocyanate (FITC)-labelled dextran (500 kDa) (TdB Consultancy, Uppsala, Sweden). A confocal microscope

 This journal is © The Royal Society of Chemistry 2025

Open Access Article. Published on 15 September 2025. Downloaded on 3/12/2026 6:43:35 PM.
This article is licensed under a Creative Commons Attribution 3.0 Unported Licence.

(Leica SP8 fitted with an HCX IRAPO L ×25 objective, CRI-U1149 Imaging Facility, Paris) was used to observe the membrane (150 μm depth was imaged with slices every 5 μm). Excitation/emission wavelengths of the live/dead assays were 490/515 nm for calcein-AM and 528/617 nm for ethidium-1.

In vivo assay

All animal procedures were performed in accordance with the National Charter and Guidelines on the Ethics of Animal Experimentation of the French National Committee for Consideration of Ethics in Animal Experimentation. The animal protocol was approved by the Local Ethical Committee and by the French Ministry of Research (authorization number: APAFIS 26843-2020080610333032V3). In total, 9 C57BL/6J mice weighing 23–28 g (Janvier, CERJ, Laval, France) were used to evaluate the tissue response after implantation in the dorsal subcutaneous space, according to ISO-10993-635.[40–42] The procedure was done under anaesthesia. For this, the anaesthesia solution was administered at 100 μL per 10 g mass of mouse. The solution contained 83.3 mg mL^{-1} ketamine (Imalgène® 500, Berial) and 3.3 mg mL^{-1} xylazine (Rompun, Bayer Health Care, Puteaux) in distilled water. Two small incisions were done on the dorsal scapular region (left and right side), and then the implants were placed in the subcutaneous space and the incision was closed using resorbable sutures. This way, each animal received two implants of 4 mm diameter PuDAlg-NaCl membrane and BioGide membrane. At the evaluation times (1, 2 and 4 weeks), animals were euthanized by overdose of ketamine/xylazine prior to tissue harvesting. For each time point, three mice have been used.

Histological analysis

Tissues surrounding the implantation area were collected and flushed with a solution of PBS 1×, followed by fixation in 4% paraformaldehyde (PFA). The fixed disks were included in the OCT compound cryostat embedding medium and sectioned with a cryotome (HM355, Microm). Tissue slides were stained with haematoxylin/eosin. Images were acquired using a high-resolution microscope (NanoZoomer S20, Hamamatsu).

Statistical analysis

Results were expressed as mean ± SD and "*n*" indicated the number of samples tested. GraphPad Prism software 8.2.1. (La Jolla, CA, USA) was used to perform the statistical analysis. A normality test was first performed using a D'Agostino & Pearson omnibus normality test. Statistical significance between several groups was assessed *via* one way analysis of variance (ANOVA), followed by a Bonferroni post-test for data assuming a Gaussian distribution. The differences for independent samples were evaluated with the nonparametric Kruskal–Wallis test and Dunn's multiple comparison test. The nonparametric Mann–Whitney test (two-tailed) was used to compare two groups. Differences were considered significant and indicated with stars when $p < 0.05$ (*), $p < 0.01$ (**), $p < 0.001$ (***), and $p < 0.0001$ (****).

Results and discussion

Topographies, barrier function and sterilisation of polysaccharide membranes

Membranes used for GTR must provide an environment for adequate tissue formation within the defect area. In guided bone formation, they must act as a barrier, preventing infiltration by non-osteogenic cells during the repair process, while allowing implant remodeling. Ideally, these membranes should feature a smooth, non-porous external surface and a rough or porous internal face that promotes integration into the defect area.

Here, three formulations based on different ratios of pullulan, dextran and alginate (PuD, PuD-NaCl and PuDAlg-NaCl) were fabricated through chemical cross-linking with STMP, and with the addition of $CaCl_2$ for the PuDAlg-NaCl. Our previous studies with PuD and PuD-NaCl hydrogels demonstrated the possibility of freeze-drying the membrane to generate a porous network. To ensure the barrier function of the membranes, a freeze-drying protocol was applied to obtain scaffolds with different faces (porous and non-porous) and inter-connected pores (Fig. 3). The surface in contact with air during the freeze-drying process was named "upper", while the surface in contact with the freeze-dryer tray was named "down".

All formulations demonstrated on the down face non-porous surfaces for cells, and open pores on the upper side. The non-porous surface of the PuD membranes presented numerous irregularities compared to the ones of PuD-NaCl and PuDAlg-NaCl that were highly homogeneous. Furthermore, cross-sectional analysis revealed that the inner porosity of the PuD membranes was homogeneous throughout its thickness. In contrast, addition of NaCl during cross-linking in PuD-NaCl membranes resulted in a gradient of the pore size as shown in the cross-section, with larger pores next to the porous surface and smaller pores next to the non-porous face. This could be due to the presence of ions during the cross-linking process that interact with the negative charges of the cross-linking bonds, tightening the polymer chains. This hypothesis is supported by a reduction of the swelling ratio from around 40 for PuD to around 5 for PuD-NaCl. Finally, the formulation of DN for PuDAlg-NaCl membranes also resulted in two different surfaces and a gradient of porosity that were characterized by larger pores next to the non-porous surface and a reduced swelling ratio (Fig. 6). As mentioned before, the presence of a gradient of pores can be beneficial in GTR. Indeed, the membrane needs to act as a barrier to avoid soft tissue ingrowth that impairs tissue regeneration while assuring good implant integration. Based on these results, PuD-NaCl and PuDAlg-NaCl seemed better suited for GTR and were therefore selected for further studies.

Analysis of the freeze-drying process can help to decipher these differences. As previously described by some of us,[43] primary nucleation, which occurs at the first step of the freeze-drying process, is a heterogeneous phenomenon. Subsequently, crystal growth occurs, dictating the final size of

Open Access Article. Published on 15 September 2025. Downloaded on 3/12/2026 6:43:35 PM.
This article is licensed under a Creative Commons Attribution 3.0 Unported Licence.

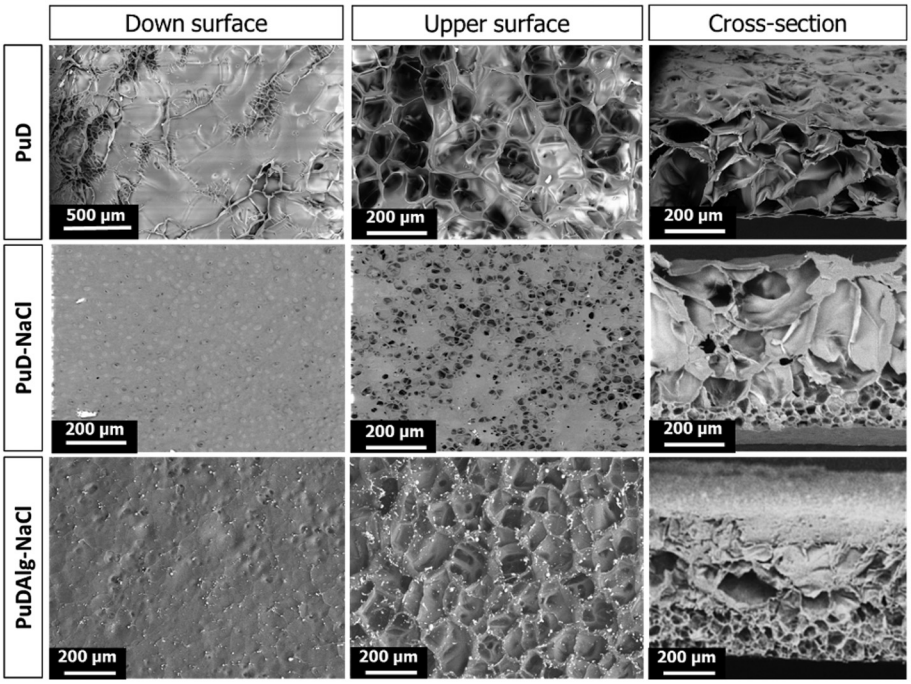

Fig. 3 Scanning electron microscopy of PuD, PuD-NaCl and PuDAlg-NaCl. Images highlighted with the absence or presence of porosities from down and upper surfaces and cross-sections. White dots on PuDAlg-NaCl membranes correspond to calcium ions. Gradient of pore sizes is visible on PuD-NaCl and PuDAlg-NaCl.

the water crystals formed within the polysaccharide hydrogel. These water crystals determine the size of the pores in the membrane following water sublimation. Control over primary nucleation can be achieved in part by regulating the kinetics and freezing temperature. Here, very small ice crystals were formed on the bottom of the membrane in contact with the freeze-dryer tray, thanks to the rapid cooling rate, leading to a smooth surface. Moreover, the gradient of pores observed in PuD-NaCl and PuDAlg-NaCl was the result of larger crystal formation leading to larger pores that facilitate the sublimation path. This crystal growth can be explained by the temperature difference between the tray and the air above the sample that facilitates the growth of crystals towards the top of the membrane. This effect is known to be dependent of the thickness of the sample. Thus, to ensure homogeneity between the samples, a tailor-made mould was used with a 300 µm-thick spacer, ensuring a consistent thickness among the batches, resulting in membranes with a final thickness of 300–400 µm after freeze-drying. The growth of the crystals from the down to the upper surfaces could also be hampered by a tighter polymer network in PuDAlg-NaCl due to the presence of the DN, resulting in polysaccharide accumulation on the upper face and thus smaller pores.

To better understand the action of the second cross-linking on the polysaccharide membranes, PuDAlg-NaCl without $CaCl_2$ were produced and compared to PuDAlg-NaCl with $CaCl_2$ cross-linking (Fig. 4). Membranes with the 2nd cross-linking presented white dots on the SEM images, revealing the presence of Ca^{2+} at the surface of the membrane. As the membranes were thoroughly rinsed before freeze-drying, the presence of salts confirmed the ionic interaction between the alginate and the cations. Regarding the intended application for GTR, we should bear in mind that the presence of Ca^{2+} could have biological applications. Indeed, it is well known that calcium ions play a crucial role in enhancing bone formation and improving osteointegration of bone implants.[44,45] In addition, SEM revealed that after the double cross-linking with $CaCl_2$ and STMP, pores seem to be interconnected as shown in Fig. 4.

Analysis of the porosity of PuD-NaCl and PuDAlg-NaCl with and without $CaCl_2$ crosslinking based on SEM images was performed (Fig. 5). An increase of pore volume was observed in PuDAlg-NaCl samples. This increase was higher for samples that did not undergo cross-linking with $CaCl_2$. Indeed, the second cross-linking with $CaCl_2$ resulted in smaller pores, proving the major role of ionic interactions in the final structure of the polymer networks. For all the formulations, the size of the pores remained compatible for cell infiltration, with pore volumes larger than the average volume of human cells (*ca.* 7×10^3 µm^3).[46]

To perform *in vitro* and *in vivo* assays, and in view of the final clinical application, membranes were exposed to UV-C light (254 nm) for 1 h, or to gamma radiation at a dose of 25 kGy used as a gold standard for medical devices. It is well known that sterilization of biomaterials may exert an influence on the chemical properties, mechanical performance, and the biological response.[47–49] UV-C light is known to have a germicidal effect when used to treat hospital surfaces,[50] and provides

 This journal is © The Royal Society of Chemistry 2025

Open Access Article. Published on 15 September 2025. Downloaded on 3/12/2026 6:43:35 PM.
This article is licensed under a Creative Commons Attribution 3.0 Unported Licence.

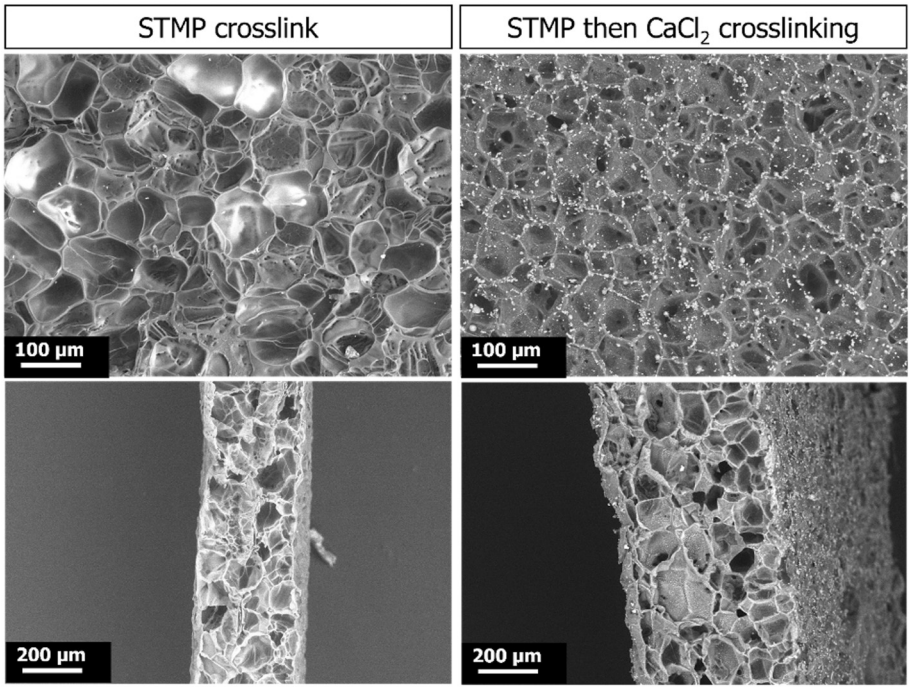

Fig. 4 SEM observations on PuDAlg-NaCl with and without $CaCl_2$ cross-linking.

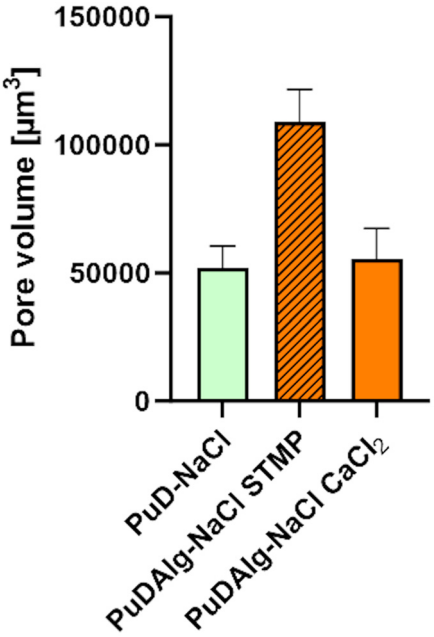

Fig. 5 Pore volume of PuD-NaCl, PuDAlg-NaCl cross-linked with STMP and PuDAlg-NaCl $CaCl_2$ cross-linked with STMP and then with $CaCl_2$.

antimicrobial activity on fresh foods,[51] food packaging[52] and vaccines.[53] Gamma rays can be applied to dry membranes and serve as a sterilization method for medical devices in industrial processess.[54] As presented in the Fig. 6, γ-rays did indeed impact the porosity of the material. In particular, the rough face appeared less homogeneous with larger pores for the PuD-NaCl formulation, while PuDAlg-NaCl seemed to present more pores. These changes are due to polysaccharide chain scissions. Indeed, γ-rays are known to degrade polysaccharides by breaking glycosidic bonds, leading to changes of the microstructure.[55,56] Although, some small pores appeared on the smooth surface, their diameter remained below 10 µm, thereby preserving the potential cell barrier effect of the material for our intended application. The PuDAlg-NaCl formulation seemed to be less impacted by sterilization.

These findings suggest that using the PuDAlg-NaCl material would allow cell penetration solely into the surface in contact with the defect site, thus promoting an effective integration of the implant while concurrently preventing undesirable migration of non-osteogenic cells into the defect.

Water uptake and degradation rate

In addition to the barrier function, a critical parameter that impacts GTR is the management of the implant by the surgeon to ensure optimal implantation and immobilization of the graft. A hydrogel which swells too much will be hard to handle and manipulate. According to the literature, DN hydrogels swell more than composite hydrogels or simple hydrogels.[27,57] Thus, the control of the swelling behaviour, and in consequence, the degradation rate of DN polysaccharide hydrogels remains a challenge.

Here, the swelling ratio of PuD-NaCl and PuDAlg-NaCl with and without the $CaCl_2$ cross-linker has been investigated as well as the enzymatic degradation (Fig. 7). First, the swelling ratio of PuDAlg-NaCl cross-linked only with STMP was 10

Open Access Article. Published on 15 September 2025. Downloaded on 3/12/2026 6:43:35 PM.
This article is licensed under a Creative Commons Attribution 3.0 Unported Licence.

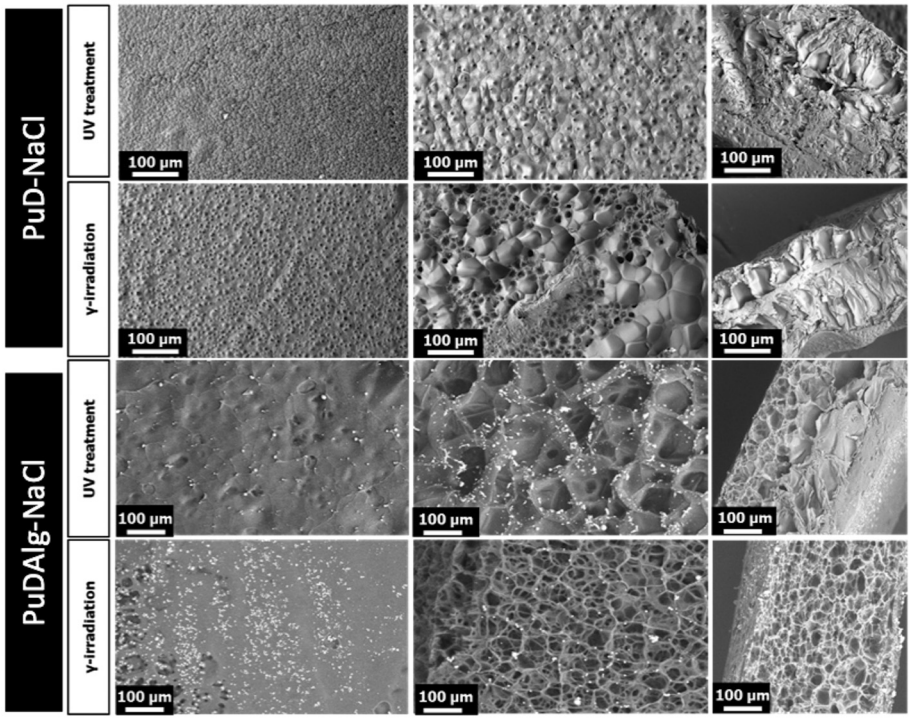

Fig. 6 Impact on the sterilisation (UV *vs.* gamma) on PuD-NaCl and PuDAlg-NaCl membranes. Observations of upper and down surfaces and cross-sections of the membranes by SEM.

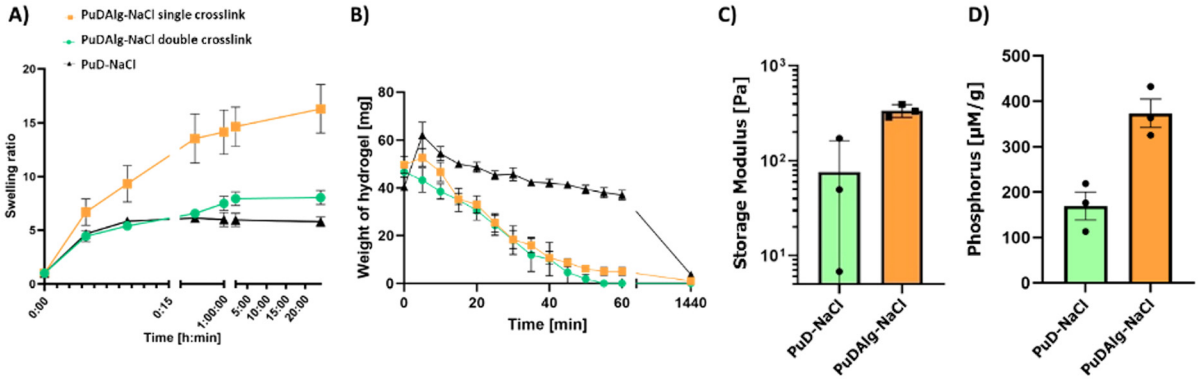

Fig. 7 (A) Swelling ratios during 24 h for PuD-NaCl; PuDAlg-NaCl crosslink with only STMP; and PuDAlg-NaCl STMP + $CaCl_2$ double crosslink. (B) Enzymatic degradation of the same three formulations for 24 h. (C and D) Structural properties of PuD-NaCl and PuDAlg-NaCl: evaluation of elastic modulus and phosphorus contents.

times higher than the swelling ratio of PuDAlg-NaCl crosslinked with STMP and $CaCl_2$, which reinforces our hypothesis that the double crosslink with Ca^{2+} increases the tightening of the network. Unexpectedly, enzymatic degradation as represented in Fig. 7B showed that PuDAlg-NaCl formulations degraded faster than PuD-NaCl. Pullulanase and dextranase are glycoside hydrolase enzymes that degrade α-1,6-glycosidic bonds in pullulan and in dextran, respectively. Since all the formulations contained the same amount of both polysaccharides and alginate, they do not present α-1,6-glycosidic linkages; this difference in degradation kinetics could not be explained by a difference in the number of cleavable bonds. Another explanation could be acid-catalysed hydrolysis mediated by carboxylic acid groups present in alginate. However, in that case, hydrolysis should be faster solely in the PuDAlg-NaCl crosslinked with only STMP, since in the presence of Ca^{2+} acid groups, neutralization takes place. Unravelling the mechanisms underlying enzymatic degradation of the membranes is beyond the scope of this work. Nevertheless, further studies should delve deeply into the degradation rate of the material using relevant *in vivo* models to contribute to tissue regeneration.[58]

 This journal is © The Royal Society of Chemistry 2025

Open Access Article. Published on 15 September 2025. Downloaded on 3/12/2026 6:43:35 PM.
This article is licensed under a Creative Commons Attribution 3.0 Unported Licence.

Mechanical properties

Rheology experiments provide information about the mechanical properties of the membrane. Due to the high-water content, the storage modulus (G') of the polysaccharide membrane could be assessed using dynamic strain sweeping performed using a rheometer. This value provides information about the viscoelasticity of materials. If G' is too low, manipulation of the membrane during implantation could be difficult, posing a problem for clinical translation. However, a high G' could be associated with low degradation rates.

To further characterize the impact of the DN on mechanical features, rheological properties were assessed on hydrated PuDAlg-NaCl and compared to hydrated PuD-NaCl membranes. Concerning the structural properties of membranes, double cross-linked PuDAlg-NaCl exhibited a higher and more homogeneous storage modulus compared to PuD-NaCl (~250 Pa for PuDAlg-NaCl *vs.* 70 Pa for PuD-NaCl), as shown in Fig. 7C. This is in accordance with an increase of the phosphorus content in PuDAlg-NaCl membranes (Fig. 7D) that proves the presence of more covalent bonds between the polysaccharide chains, resulting in the stiffening of the membranes. This difference could thus be attributed to different cross-linking rates of the membranes and higher tightening of the network with more phosphate groups (Fig. 7). To note, these rheological studies were performed to mimic the act of

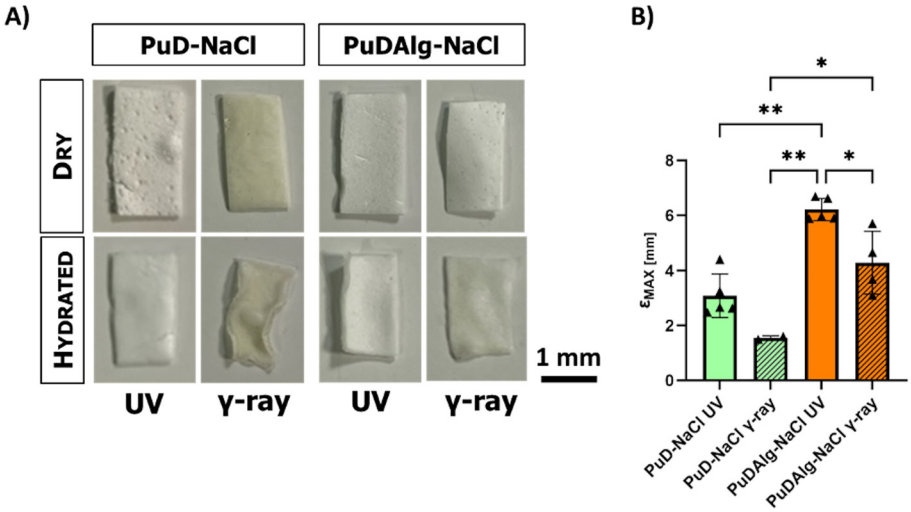

Fig. 8 Elongation studies on PuD-NaCl and PuDAlg-NaCl irradiated with UV or gamma rays. (A) Aspect of the membranes 5 minutes after hydration. (B) Maximum elongation of the membranes.

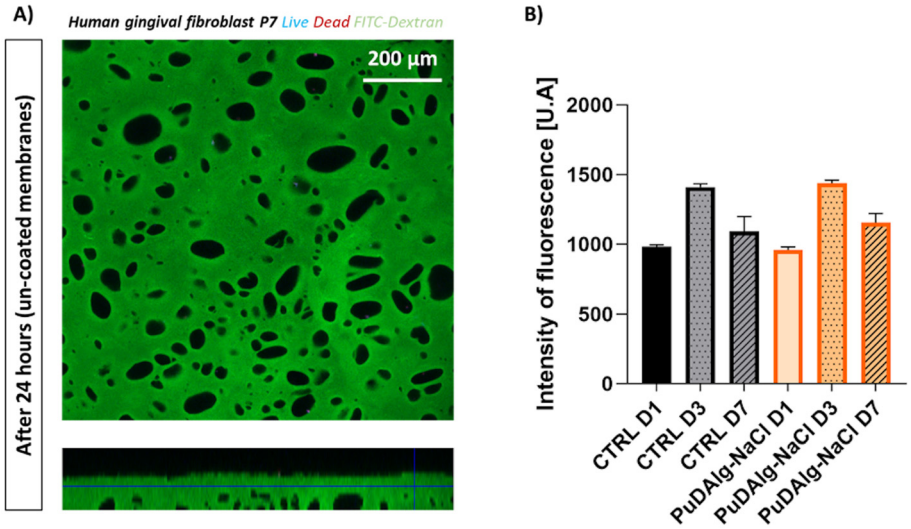

Fig. 9 (A) Barrier effect observed by confocal analysis at day 1 performed with human gingival fibroblasts seeded on the smooth surface. Absence of cells inside pores indicated that no infiltration nor migration has occurred. (B) Indirect cell viability on PuDAlg-NaCl up to 7 days.

Open Access Article. Published on 15 September 2025. Downloaded on 3/12/2026 6:43:35 PM.
This article is licensed under a Creative Commons Attribution 3.0 Unported Licence.

surgery with membranes that were hydrated for only 5 min, and not fully swollen. Totally swollen membranes with a higher swelling ratio, like PuDAlg-NaCl, are expected to present a lower elastic modulus value in the swollen state.

As mentioned, increasing the number of phosphate bonds in the PuDAlg-NaCl formulation led to a more rigid membrane. The addition of alginate in the formulation also allowed the creation of new bonds with $CaCl_2$ in order to develop a more complex and resistant network but one that is still reversible. These results align with those of previous studies with polysaccharide hydrogels[59] and correspond to elastic properties within the range of human soft tissues.[60–62]

Considering the intended application for GTR, we were interested in assessing the suturability and immobilization of

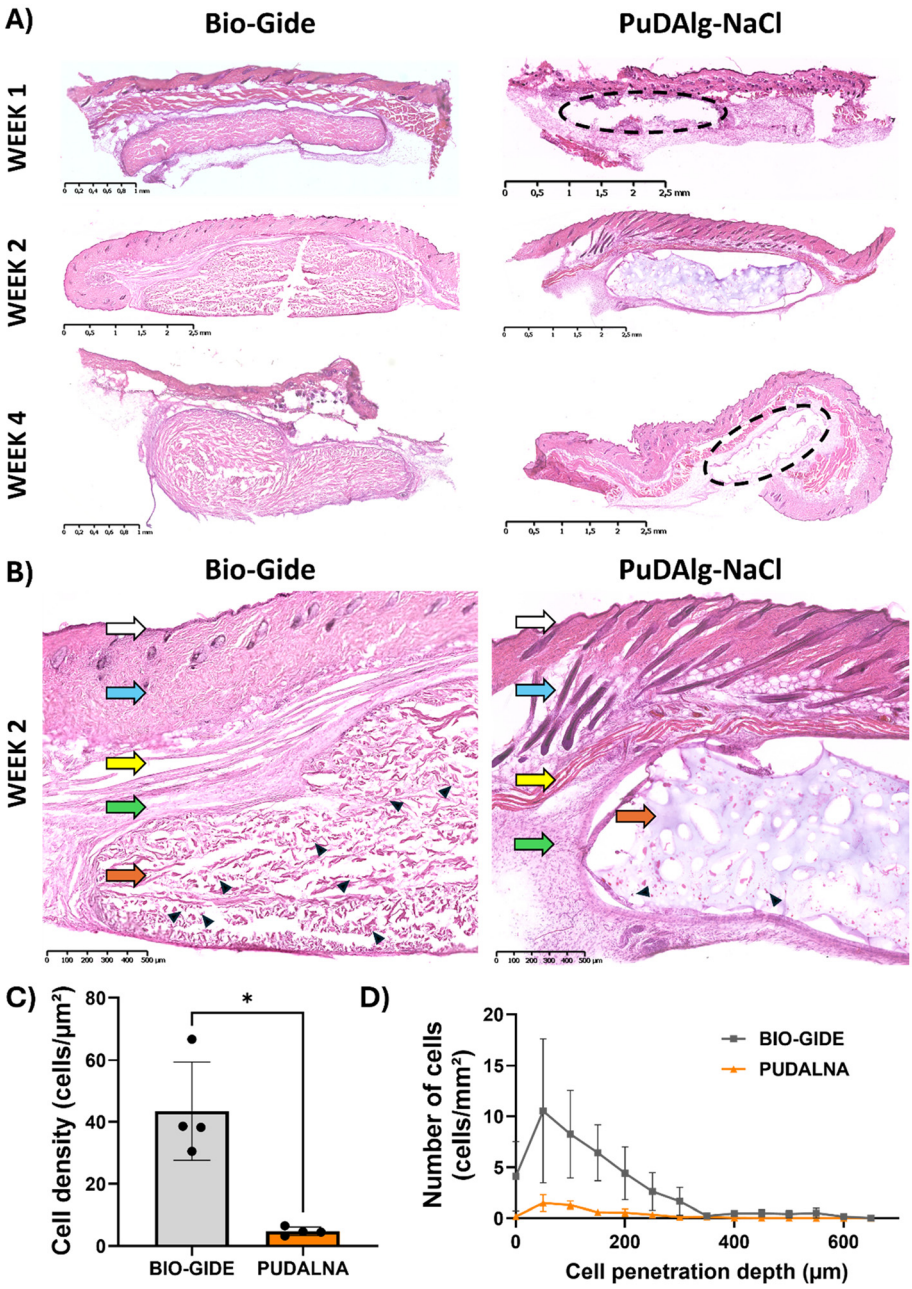

Fig. 10 *In vivo* subcutaneous implantation of gamma-ray-sterilised PuDAlg-NaCl membranes and commercialized Bio-Gide collagen membranes as the control. (A) Haematoxylin–eosin staining after 1, 2 or 4 weeks of implantation. The PuDAlg-NaCl membrane was lost during the staining for week 1 and week 4 samples. The initial positions of the membranes are surrounded by dotted lines. (B) Higher magnification images of the week 2 samples are presented in (A). The arrows indicate the epidermis (white arrows), the dermis (blue arrows), the muscular layer (yellow arrows), the fibrous capsule (green arrows), the implanted biomaterial (orange arrows) and the cell present in the biomaterial (black arrowheads). (C) Quantification of the cell density in the biomaterial membrane, either Bio-Gide or PuDAlg-NaCl after 2 weeks of implantation. (D) Evaluation of the cell penetration depth for the Bio-Gide and the PuDAlg-NaCl samples after 2 weeks of implantation, measured on 4 distinct slides.

Open Access Article. Published on 15 September 2025. Downloaded on 3/12/2026 6:43:35 PM.
This article is licensed under a Creative Commons Attribution 3.0 Unported Licence.

the membrane at the defect site. Creep tests using sutures were conducted using PuD-NaCl and PuDAlg-NaCl. In view of clinical applications, membranes after sterilization were also studied. To simulate the surgical act of implantation, the samples were hydrated for 5 min, and then tensile testing was performed by applying 30% strain until rupture occurred. Maximum elongation was achieved with a displacement mode test and without preload. The results, depicted in Fig. 8, show higher deformation of UV-treated samples prior to rupture for both PuD-NaCl and PuDAlg-NaCl. Although manipulation of gamma-irradiated membranes was challenging due to shrinking of the material (Fig. 8A), PuDAlg-NaCl showed higher maximum elongation than PuD-NaCl (Fig. 8B), which confirmed enhanced properties for GTR applications. Following mechanical and structural results, the PuDAlg-NaCl membrane was selected for further investigation *in vitro* and *in vivo*.

In vitro results

The barrier effect of the membrane, attributed to obtaining a smooth non-porous surface, was confirmed by cell seeding of human gingival fibroblasts on top of the non-porous face. After 24 h, no cells were present on the surface with absence of migration throughout the membrane thickness (Fig. 9A). Cell seeding was also performed on the rough side (Fig. S1†), demonstrating that cells could penetrate through the pores on the surface, although they did not adhere and remained spherical due to lack of cell adhesion motifs on the polysaccharide chains. This is consistent with our previous works, in which pullulan–dextran hydrogels were used to induce autoassembly of spheroids, thanks to the absence of cell–matrix interactions that favoured cell–cell interactions.[12,61] Moreover, we have also demonstrated that by adding ECM proteins on the surface of the pores, such as collagen and laminin, cells adhered and were able to proliferate and migrate within the pore network.[13,61] This absence of cell adhesion prompted the selection of an indirect assay to assess cytotoxicity. Consequently, a metabolic assay was conducted using fibroblasts cultured in the conditioned medium obtained after 7 days of incubation with the membranes. Results indicate that PuDAlg-NaCl exhibited no cytotoxicity (Fig. 9B), highlighting that the absence of cells was due to the absence of coating and not due to toxicity from the material itself.

In vivo results

For the *in vivo* studies, gamma-irradiated PuDAlg-NaCl samples were used and compared with the commercialised material (Bio-Gide) as the control, in terms of the cell penetration, the inflammatory response and degradation behaviour. Subcutaneous implantation of the two types of membranes was feasible, and the implants remained at the site of implantation during the entire 4-week study period. Tissue response and material behaviour was studied through haematoxylin–eosin staining of the implants and the surrounding tissue.

One week after implantation, the tissue surrounding PuDAlg-NaCl exhibited mild inflammation, which was reduced after 2 weeks, when an incipient fibrotic capsule surrounding the implants was detected (Fig. 10A and B). This is in line with other studies that showed peak inflammatory responses appearing during the first 7 days after implantation.[63–66] After two and four weeks, the PuDAlg-NaCl membrane did not induce any chronic inflammation, as evidenced by the absence of macrophages and Langerhans cells. Generally, the surface chemistry of the biomaterials is involved in protein absorption, leading to acute or chronic inflammation, with the apparition of fibrotic encapsulation. Alginate is well known for presenting low immunogenicity, especially low molecular weight alginate.[67] Moreover, studies have shown that alginate can modulate the release of pro-inflammatory cytokines, leading to a more favourable healing environment.[68]

An interesting outcome was the effective barrier effect achieved with the polysaccharide membrane. Although some cells could invade the pores of the membrane (Fig. 10B), cell density and penetration depth were both reduced compared to the Bio-Gide membrane, currently used in the clinic (Fig. 10C and D). The remodelling and biodegradability of polysaccharide membranes was visible after two weeks, whereas the Bio-Gide collagen membrane remained perfectly intact over the month of implantation. When using polysaccharide membranes, this could be advantageous for bone regeneration in small defects within the oral cavity that typically occurs within the first 2–6 months post-implantation.[69,70] Ideally, material resorption should occur within a similar timeframe to facilitate optimal healing. To completely assess the resorption while the regeneration occurs, further studies of PuDAlg-NaCl when simulating clinical conditions should be performed on larger animals.

Conclusions

The objective of this study was to develop a polysaccharide-based animal-free biodegradable membrane tailored for GTR combining desirable physical, biological, and mechanical properties. By formulating a double-network hydrogel composed of pullulan, dextran, and alginate, cross-linked with STMP and $CaCl_2$, we achieved a membrane with enhanced mechanical integrity suitable for GTR. In conjunction with previous research demonstrating osteoinductive properties of pullulan–dextran-hydroxyapatite beads, these results lay the groundwork for evaluating the efficacy of polysaccharide membranes in treating oral bone defects in combination with a bone filler.

Data availability

The data collected throughout the course of this study are presented and detailed within the main sections of the manuscript.

Open Access Article. Published on 15 September 2025. Downloaded on 3/12/2026 6:43:35 PM.
This article is licensed under a Creative Commons Attribution 3.0 Unported Licence.

Conflicts of interest

There are no conflicts of interest to declare.

Acknowledgements

This project has received funding from the H2020-NMBP-HUBS-2018 TBMED project: Grant Agreement No. 814439 and from the Agence Nationale de la Recherche GlycoMB grant number ANR-20-CE18-0034. The authors gratefully acknowledge the Photonic Imaging Platform IMA'CRI (Centre de recherche sur l'Inflammation – CRI, INSERM) and the ImagoSeine core facility of the Institut Jacques Monod, member of the France BioImaging infrastructure (ANR-10-INBS-04) and GIS-IBiSA, and support of the Region Île-de-France (Sesame).

References

1 P. Gentile, V. Chiono, C. Tonda-Turo, A. M. Ferreira and G. Ciardelli, Polymeric membranes for guided bone regeneration, *Biotechnol. J.*, 2011, 1187–1197.
2 J. Wang, L. Wang, Z. Zhou, H. Lai, P. Xu, L. Liao, *et al.*, Biodegradable Polymer Membranes Applied in Guided Bone/Tissue Regeneration: A Review, *Polymers*, 2016, **8**, 115.
3 R. A. Namanloo, M. Ommani, K. Abbasi, M. Alam, A. Badkoobeh, M. Rahbar, *et al.*, Biomaterials in Guided Bone and Tissue Regenerations: An Update, Chen Q, éditeur, *Adv. Mater. Sci. Eng.*, 2022, 1–14.
4 D. Sanjanwala, V. Londhe, R. Trivedi, S. Bonde, S. Sawarkar, V. Kale, *et al.*, Polysaccharide-based hydrogels for medical devices, implants and tissue engineering: A review, *Int. J. Biol. Macromol.*, 2024, **256**, 128488.
5 C. Su, Y. Chen, S. Tian, C. Lu and Q. Lv, Research Progress on Emerging Polysaccharide Materials Applied in Tissue Engineering, *Polymers*, 2022, 3268.
6 T. Miao, J. Wang, Y. Zeng, G. Liu and X. Chen, Polysaccharide–Based Controlled Release Systems for Therapeutics Delivery and Tissue Engineering: From Bench to Bedside, *Adv. Sci.*, 2018, 1700513.
7 J. E. Smith, R. Sullivan and N. J. Rowan, The Role of Polysaccharides Derived from Medicinal Mushrooms in Cancer Treatment Programs: Current Perspectives (Review), *Int. J. Med. Mushrooms*, 2003, **8**, 18.
8 C. Buckley, E. J. Murphy, T. R. Montgomery and I. Major, Hyaluronic Acid: A Review of the Drug Delivery Capabilities of This Naturally Occurring Polysaccharide, *Polymers*, 2022, 3442.
9 S. Tiwari, R. Patil and P. Bahadur, Polysaccharide Based Scaffolds for Soft Tissue Engineering Applications, *Polymers*, 2018, 1.
10 C. Dujardin, W. Habeler, C. Monville, D. Letourneur and T. Simon-Yarza, Advances in the engineering of the outer blood-retina barrier: From *in vitro* modelling to cellular therapy, *Bioact. Mater.*, 2024, 151–177.
11 A. Dellaquila, C. Dujardin, C. Le Bao, C. Chaumeton, A. Carré and C. Le Guilcher, Fibroblasts mediate endothelium response to angiogenic cues in a newly developed 3D stroma engineered model, *Biomater. Adv.*, 2023, 213636.
12 M. N. Labour, C. Le Guilcher, R. Aid-Launais, N. El Samad, S. Lanouar, T. Simon-Yarza, *et al.*, Development of 3D Hepatic Constructs Within Polysaccharide-Based Scaffolds with Tunable Properties, *Int. J. Mol. Sci.*, 2020, 3644.
13 T. Simon-Yarza, M. N. Labour, R. Aid and D. Letourneur, Channeled polysaccharide-based hydrogel reveals influence of curvature to guide endothelial cell arrangement in vessel-like structures, *Mater. Sci. Eng., C*, 2021, **118**, 111369.
14 J. C. Fricain, S. Schlaubitz, C. Le Visage, I. Arnault, S. M. Derkaoui, R. Siadous, *et al.*, A nano-hydroxyapatite – Pullulan/dextran polysaccharide composite macroporous material for bone tissue engineering, *Biomaterials*, 2013, 2947–2959.
15 N. Ahmed Omar, J. Roque, P. Galvez, R. Siadous, O. Chassande, S. Catros, *et al.*, Development of Novel Polysaccharide Membranes for Guided Bone Regeneration: In Vitro and In Vivo Evaluations, *Bioengineering*, 2023, 1257.
16 P. Aprile, D. Letourneur and T. Simon-Yarza, Membranes for Guided Bone Regeneration: A Road from Bench to Bedside, *Adv. Healthcare Mater.*, 2020, 2000707.
17 M. Jin, J. Shi, W. Zhu, H. Yao and D. A. Wang, Polysaccharide-Based Biomaterials in Tissue Engineering: A Review, *Tissue Eng., Part B*, 2021, 604–626.
18 N. B. Shelke, R. James, C. T. Laurencin and S. G. Kumbar, Polysaccharide biomaterials for drug delivery and regenerative engineering, *Polym. Adv. Technol.*, 2014, 448–460.
19 S. Babu, A. Shanmugavadivu and N. Selvamurugan, Tunable mechanical properties of chitosan-based biocomposite scaffolds for bone tissue engineering applications: A review, *Int. J. Biol. Macromol.*, 2024, 132820.
20 R. F. Bombaldi De Souza, F. C. Bombaldi De Souza, C. Rodrigues, B. Drouin, K. C. Popat, D. Mantovani, *et al.*, Mechanically-enhanced polysaccharide-based scaffolds for tissue engineering of soft tissues, *Mater. Sci. Eng., C*, 2019, 364–375.
21 F. Lee and M. Kurisawa, Formation and stability of interpenetrating polymer network hydrogels consisting of fibrin and hyaluronic acid for tissue engineering, *Acta Biomater.*, 2013, 5143–5152.
22 C. O. Crosby, B. Stern, N. Kalkunte, S. Pedahzur, S. Ramesh and J. Zoldan, Interpenetrating polymer network hydrogels as bioactive scaffolds for tissue engineering, *Rev. Chem. Eng.*, 2022, 347–361.
23 C. E. Vorwald, T. Gonzalez-Fernandez, S. Joshee, P. Sikorski and J. K. Leach, Tunable fibrin-alginate interpenetrating network hydrogels to support cell spreading and network formation, *Acta Biomater.*, 2020, 142–152.
24 X. Hou, L. Lin, K. Li, F. Jiang, D. Qiao, B. Zhang, *et al.*, Towards superior biopolymer gels by enabling interpene-

 This journal is © The Royal Society of Chemistry 2025

Open Access Article. Published on 15 September 2025. Downloaded on 3/12/2026 6:43:35 PM.
This article is licensed under a Creative Commons Attribution 3.0 Unported Licence.

trating network structures: A review on types, applications, and gelation strategies, *Adv. Colloid Interface Sci.*, 2024, 103113.

25 P. Karami, C. S. Wyss, A. Khoushabi, A. Schmocker, M. Broome, C. Moser, *et al.*, Composite Double-Network Hydrogels To Improve Adhesion on Biological Surfaces, *ACS Appl. Mater. Interfaces*, 2018, 38692–38699.

26 H. Kichi, T. Nakajima, T. Matsuda, T. Sakai and J. P. Gong, Network elasticity of a model hydrogel as a function of swelling ratio: from shrinking to extreme swelling states, *Soft Matter*, 2018, 9693–9701.

27 C. S. Wyss, Hybrid hydrogels for load-bearing implants, PhD Thesis, EPFL, 2021, 211.

28 H. Shin, B. D. Olsen and A. Khademhosseini, The mechanical properties and cytotoxicity of cell-laden double-network hydrogels based on photocrosslinkable gelatin and gellan gum biomacromolecules, *Biomaterials*, 2012, 3143–3152.

29 S. A. Young, H. Riahinezhad and B. G. Amsden, *In situ* -forming, mechanically resilient hydrogels for cell delivery, *J. Mater. Chem. B*, 2019, 5742–5761.

30 Q. Gao, B. S. Kim and G. Gao, Advanced Strategies for 3D Bioprinting of Tissue and Organ Analogs Using Alginate Hydrogel Bioinks, *Mar. Drugs*, 2021, 708.

31 M. F. Moradali, S. Ghods and B. H. A. Rehm, Alginate Biosynthesis and Biotechnological Production, in *Springer Series in Biomaterials Science and Engineering*, ed. B. H. A. Rehm and M. F. Moradali, 2018, vol. 11, pp. 1–25.

32 A. Abed, N. Assoul, M. Ba, S. M. Derkaoui, P. Portes, L. Louedec, *et al.*, Influence of polysaccharide composition on the biocompatibility of pullulan/dextran–based hydrogels, *J. Biomed. Mater. Res., Part A*, 2011, 535–542.

33 S. Tanveer and C. C. Chen, Thermodynamic analysis of hydrogel swelling in aqueous sodium chloride solutions, *J. Mol. Liq.*, 2022, 118421.

34 M. Lavergne, M. Derkaoui, C. Delmau, D. Letourneur, G. Uzan and C. Le Visage, Porous Polysaccharide–Based Scaffolds for Human Endothelial Progenitor Cells, *Macromol. Biosci.*, 2012, 901–910.

35 D. Bruneel and E. Schacht, Enzymatic Degradation of Pullulan and Pullulan Derivatives, *J. Bioact. Compat. Polym.*, 1995, 299–312.

36 S. Lanouar, R. Aid-Launais, A. Oliveira, L. Bidault, B. Closs, M. N. Labour, *et al.*, Effect of cross-linking on the physicochemical and in vitro properties of pullulan/dextran microbeads, *J. Mater. Sci. Mater. Med.*, 2018, 77.

37 T. G. Mezger, in *Rhéologie appliquée: à la découverte de la rhéologie avec Joe Flow*, 2017.

38 N. A. Peppas and E. W. Merrill, Crosslinked poly(vinyl alcohol) hydrogels as swollen elastic networks, *J. Appl. Polym. Sci.*, 1977, 1763–1770.

39 International Organization for Standardization. ISO 10993-5:2009(en), Biological evaluation of medical devices—Part 5: Tests for in vitro cytotoxicity, 2009.

40 R. C. Rennert, M. Sorkin, R. K. Garg, M. Januszyk and G. C. Gurtner, Cellular Response to a Novel Fetal Acellular Collagen Matrix: Implications for Tissue Regeneration, *Int. J. Biomater.*, 2013, 1–9.

41 J. R. Sarkanen, V. Kaila, B. Mannerström, S. Räty, H. Kuokkanen, S. Miettinen, *et al.*, Human adipose tissue extract induces angiogenesis and adipogenesis in vitro, *Tissue Eng., Part A*, 2012, 17–25.

42 W. M. L. Neethling, R. Glancy and A. J. Hodge, Mitigation of calcification and cytotoxicity of a glutaraldehyde-preserved bovine pericardial matrix: improved biocompatibility after extended implantation in the subcutaneous rat model, *J. Heart Valve Dis.*, 2010, 778–785.

43 J. Grenier, H. Duval, F. Barou, P. Lv, B. David and D. Letourneur, Mechanisms of pore formation in hydrogel scaffolds textured by freeze-drying, *Acta Biomater.*, 2019, 195–203.

44 J. Jeong, J. H. Kim, J. H. Shim, N. S. Hwang and C. Y. Heo, Bioactive calcium phosphate materials and applications in bone regeneration, *Biomater. Res.*, 2019, 4.

45 M. N. Lee, H. S. Hwang, S. H. Oh, A. Roshanzadeh, J. W. Kim, J. H. Song, *et al.*, Elevated extracellular calcium ions promote proliferation and migration of mesenchymal stem cells via increasing osteopontin expression, *Exp. Mol. Med.*, 2018, 1–16.

46 G. B. Carr and C. A. F. Murgel, The Use of the Operating Microscope in Endodontics, *Dent. Clin. North Am.*, 2010, 191–214.

47 Y. S. Tapia-Guerrero, M. L. Del Prado-Audelo, F. V. Borbolla-Jiménez, D. M. Giraldo Gomez, I. García-Aguirre, C. A. Colín-Castro, *et al.*, Effect of UV and Gamma Irradiation Sterilization Processes in the Properties of Different Polymeric Nanoparticles for Biomedical Applications, *Materials*, 2020, 1090.

48 A. L. Santos, V. Oliveira, I. Baptista, I. Henriques, N. C. M. Gomes, A. Almeida, *et al.*, Wavelength dependence of biological damage induced by UV radiation on bacteria, *Arch. Microbiol.*, 2013, 63–74.

49 G. Horneck, in *UV Radiation, Biological Effects*, ed. M. Gargaud, W. M. Irvine, R. Amils, H. J. Cleaves, D. L. Pinti, J. C. Quintanilla, *et al.*, 2015, pp. 2577–2580.

50 J. H. Yang, U. I. Wu, H. M. Tai and W. H. Sheng, Effectiveness of an ultraviolet-C disinfection system for reduction of healthcare-associated pathogens, *J. Microbiol., Immunol. Infect.*, 2019, 487–493.

51 V. Yemmireddy, A. Adhikari and J. Moreira, Effect of ultraviolet light treatment on microbiological safety and quality of fresh produce: An overview, *Front. Nutr.*, 2022, 871243.

52 I. Racchi, N. Scaramuzza, A. Hidalgo, M. Cigarini and E. Berni, Sterilization of food packaging by UV-C irradiation: Is Aspergillus brasiliensis ATCC 16404 the best target microorganism for industrial bio-validations?, *Int. J. Food Microbiol.*, 2021, 109383.

53 A. Vrablikova, M. Fojtikova, R. Hezova, P. Simeckova, V. Brezani, N. Strakova, *et al.*, UV-C irradiation as an effective tool for sterilization of porcine chimeric VP1-PCV2bCap recombinant vaccine, *Sci. Rep.*, 2023, 19337.

Open Access Article. Published on 15 September 2025. Downloaded on 3/12/2026 6:43:35 PM.
This article is licensed under a Creative Commons Attribution 3.0 Unported Licence.

54 C. C. Beh, Sterilization Techniques of Biomaterials (Implants and Medical Devices), in *Biomaterials and Biopolymers*, ed. A. Domb, B. Mizrahi and S. Farah, 2023, pp. 255–269.
55 J. M. Wasikiewicz, F. Yoshii, N. Nagasawa, R. A. Wach and H. Mitomo, Degradation of chitosan and sodium alginate by gamma radiation, sonochemical and ultraviolet methods, *Radiat. Phys. Chem.*, 2005, 287–295.
56 Y. S. Hamed, K. R. Hassan, M. E. Salem, M. Shen, J. Wang, T. Bu, *et al.*, Gamma rays irradiated polysaccharides: A review of the structure, physicochemical properties, biological activities alteration, and future food applications, *Carbohydr. Polym.*, 2025, 123326.
57 C. S. Wyss, P. Karami, P. E. Bourban and D. P. Pioletti, Hybrid granular hydrogels: combining composites and microgels for extended ranges of material properties, *Soft Matter*, 2020, 3769–3778.
58 L. Guangyuan, S. Baiyang, W. Gan, W. Yujun, G. Yandao, Z. Xiufang, *et al.*, Controlling the Degradation of Covalently Cross-linked Carboxymethyl Chitosan Utilizing Bimodal Molecular Weight Distribution, *J. Biomater. Appl.*, 2009, 435–451.
59 J. Grenier, H. Duval, P. Lv, F. Barou, C. Le Guilcher, R. Aid, *et al.*, Interplay between crosslinking and ice nucleation controls the porous structure of freeze-dried hydrogel scaffolds, *Biomater. Adv.*, 2022, 212973.
60 C. F. Guimarães, L. Gasperini, A. P. Marques and R. L. Reis, The stiffness of living tissues and its implications for tissue engineering, *Nat. Rev. Mater.*, 2020, 351–370.
61 C. Le Guilcher, G. Merlen, A. Dellaquila, M. N. Labour, R. Aid, T. Tordjmann, *et al.*, Engineered human liver based on pullulan-dextran hydrogel promotes mice survival after liver failure, *Mater. Today Bio*, 2023, 100554.
62 A. Dellaquila, C. Dujardin, C. Le Bao, C. Chaumeton, A. Carré, C. Le Guilcher, *et al.*, Fibroblasts mediate endothelium response to angiogenic cues in a newly developed 3D stroma engineered model, *Biomater. Adv.*, 2023, 213636.
63 L. Tang, T. A. Jennings and J. W. Eaton, Mast cells mediate acute inflammatory responses to implanted biomaterials, *Proc. Natl. Acad. Sci. U. S. A.*, 1998, 8841–8846.
64 L. Tang and J. W. Eaton, Inflammatory Responses to Biomaterials, *Am. J. Clin. Pathol.*, 1995, 466–471.
65 F. Boccafoschi, C. Mosca and M. Cannas, Cardiovascular biomaterials: when the inflammatory response helps to efficiently restore tissue functionality?: Inflammatory response to cardiovascular biomaterials, *J. Tissue Eng. Regener. Med.*, 2014, 253–267.
66 G. Zhou and T. Groth, Host Responses to Biomaterials and Anti–Inflammatory Design—a Brief Review, *Macromol. Biosci.*, 2018, 1800112.
67 X. Xu, D. Bi and M. Wan, Characterization and Immunological Evaluation of Low-Molecular- Weight Alginate Derivatives, *Curr. Top. Med. Chem.*, 2015, 874–887.
68 J. W. Lamppa and K. E. Griswold, Alginate Lyase Exhibits Catalysis-Independent Biofilm Dispersion and Antibiotic Synergy, *Antimicrob. Agents Chemother.*, 2013, 137–145.
69 R. Sharma, P. K. Sharma and R. Malviya, Polysaccharide-based Scaffolds for Bone Marrow Regeneration: Recent Work and Commercial Utility (Patent), *Curr. Smart Mater.*, 2019, 29–35.
70 J. Venkatesan, S. Anil, S. Rao, I. Bhatnagar and S. K. Kim, Sulfated Polysaccharides from Macroalgae for Bone Tissue Regeneration, *Curr. Pharm. Des.*, 2019, 1200–1209.

 This journal is © The Royal Society of Chemistry 2025